

## Article

# Comparative Study of TiMn and TiAlV Alloys via the Nanoindentation Technique

Shafaq Asrar <sup>1</sup>, Ambreen Azmat <sup>1</sup>, Iftikhar Ahmed Channa <sup>2</sup>, Jaweria Ashfaq <sup>2</sup>, Faraz Sufyan <sup>3</sup>, Sarmad Feroze <sup>4</sup>, Ali Dad Chandio <sup>1,2,\*</sup>, Muhammad Ali Shar <sup>5</sup> and Abdulaziz Alhazaa <sup>6</sup>

<sup>1</sup> Materials and Surface Engineering Research Lab, Department of Metallurgical Engineering, NED University of Engineering and Technology, Karachi 75270, Pakistan

<sup>2</sup> Thin Film Lab, Department of Metallurgical Engineering, NED University of Engineering and Technology, Karachi 75270, Pakistan

<sup>3</sup> Department of Petroleum Technology, University of Karachi, Karachi 75270, Pakistan

<sup>4</sup> Solar Factory of the Future, Bavarian Center for Applied Energy Research (ZAE Bayern), Fürther Straße 250, 90429 Nürnberg, Germany

<sup>5</sup> Department of Mechanical & Energy Systems Engineering, Faculty of Engineering and Informatics, University of Bradford, Bradford BD7 1DP, UK

<sup>6</sup> Department of Physics and Astronomy, College of Science, King Saud University, Riyadh 11451, Saudi Arabia

\* Correspondence: alidad@neduet.edu.pk



**Citation:** Asrar, S.; Azmat, A.; Channa, I.A.; Ashfaq, J.; Sufyan, F.; Feroze, S.; Chandio, A.D.; Ali Shar, M.; Alhazaa, A. Comparative Study of TiMn and TiAlV Alloys via the Nanoindentation Technique. *Crystals* **2022**, *12*, 1537. <https://doi.org/10.3390/crust12111537>

Academic Editor: Per-Lennart Larsson

Received: 3 October 2022

Accepted: 21 October 2022

Published: 28 October 2022

**Publisher's Note:** MDPI stays neutral with regard to jurisdictional claims in published maps and institutional affiliations.



**Copyright:** © 2022 by the authors. Licensee MDPI, Basel, Switzerland. This article is an open access article distributed under the terms and conditions of the Creative Commons Attribution (CC BY) license (<https://creativecommons.org/licenses/by/4.0/>).

**Abstract:** There are two common categories of implants that are used in medical sciences, i.e., orthopedic and dental ones. In this study, dental implant materials are focused such as Ti6Al4V alloys that are used for the replacement of lost teeth due to their high strength and biocompatibility. However, they cause infections in nearby tissues due to elemental release (potentially Al and V). Thus, manganese is selected to be incorporated into the alloy since it is also present in the human body in the form of traces. Different sets of implants were produced, i.e., Ti5Mn and Ti10Mn (where 5 and 10 describe the percentage of Mn) by using the powder metallurgy technique. This was followed by characterization techniques, including X-ray fluorescence spectroscopy (XRF), X-ray diffractometer (XRD), optical microscope (OM), and nanoindenter. The very aim of this study is to compare the microstructural evolutions, density, and mechanical properties of reference alloys and the ones produced in this study. Results show the microstructure of Ti6Al4V consists of the alpha ( $\alpha$ ) and beta ( $\beta$ ) phases, while Ti5Mn and Ti10Mn revealed the beta ( $\beta$ ) phases. The Ti5Mn alloy showed excellent mechanical properties than that of the Ti6Al4V counterpart. Extensive discussion is presented in light of the observed results. The relative density of Ti5Mn alloy was found to be enhanced than that of reference alloy.

**Keywords:** Ti6Al4V; Ti-5Mn; Ti-10Mn; hardness; elastic modulus; dental implants

## 1. Introduction

Titanium (Ti) and the alloys based on it are a superb choice for implant applications, owing to their mechanical characteristics, as well as those deliberated by the surface, i.e., resistance to corrosion and bioactivity [1]. The vital features of Ti-alloys which make them ideal alternate for biomedical applications include their light weight, good mechanical strength, high resistance to corrosion, excellent biocompatibility, nonmagnetic characteristics, and comparatively low modulus of elasticity [2,3]. However, Ti6Al4V alloy is made out of cytotoxic elements, such as aluminum (Al) and vanadium (V), that may cause extreme issues once delivered to the human body. The reason behind the cytotoxicity of aluminum and vanadium is that the living body is an aggressive environment composed of water, saliva, complex organic compounds, plasma, lymph, and different types of ions that electrochemically react with the implant and cause corrosion. Previous research shows that vanadium ions release from alloys within the human body via a passive dissolution

mechanism that causes discoloration of the neighboring tissue or produces an inflammatory reaction that is the reason of discomfort and may cause loosening of the implant due to osteolysis [4].

Moreover, Al reveals only a single oxidation state, i.e.,  $\text{Al}^{3+}$ , which has negative chemical affinity, and it behaves like an oxygen-donor ligand. Various complex compounds that contain carboxylate, inorganic, deprotonated hydroxyl, and organic phosphates groups form strong chemical bonds with  $\text{Al}^{3+}$ . Due to this chemical behavior,  $\text{Al}^{3+}$  forms bonds to the phosphate groups of DNA and RNA, disturbing the DNA chemical structure and manipulating the appearance of several genes crucial for brain roles [5].

To beat the possible aluminum and vanadium toxic effect, it was replaced by manganese (Mn), prompting the formation of a new V-free titanium-based alloy [6]. As a stable component, Mn influenced the  $\beta$  phase with a strong solid solution strengthening effect. Mn, as a trace element, assumes a significant part in maintaining normal metabolism [7]. Manganese was selected due to minimal cost, capacity to enhance the mechanical characteristics of titanium through the development of two-stage microstructures, and connection with the living body. Mn supports [8] bone growth and stimulates several vital enzyme systems and due to this ability, it is a requisite for the synthesis of acid mucopolysaccharides, such as chondroitin sulfate, to produce the matrices of bones. Moreover, manganese plays the role of a co-factor in the production of bone cartilage and collagen, as well as in bone mineralization [9]. Thus, in comparison to other  $\beta$  stabilizers, the Mn, which is naturally available in large quantities, has a lower toxic effect and lower cost [10,11].

Consequently, it is significant to compare the mechanical properties of Ti6Al4V, Ti5Mn, and Ti10Mn alloys. While ordinary testing strategies are generally utilized for estimating the mechanical properties of bulk materials, for ordinary specimen geometries, such as small sample sizes or rough shapes, which are difficult to test, nanoindentation is a grounded strategy for estimating the mechanical characteristics of a varied scope of materials particularly when a nondestructive methodology is mandatory [12].

Lately, the nanoindentation strategy has been introduced as an option in contrast to the regular testing strategies, since it is straightforward, quick, nondestructive, generally cheap, and requires a small size of the specimen [13–16].

Nanoindentation has been a progressively current technique for material characterization on a nanoscale [17] due to its high spatial and depth resolution of the measurement [18]. Several mechanical properties of a coating/substrate system may be acquired using the nanoindentation technique. Due to its high hardness and elastic modulus diamond is often used as a tip of the indenter [19].

A characteristic measurement that a nanoindenter can record is the displacement ( $h$ ) from the material surface in sub-nm and load ( $P$ ) in sub-mN. From the documented  $P$  vs.  $h$  curve, several characteristics of the material, such as the yield strength, elastic modulus, residual stress, hardness, fracture toughness, and strain hardening exponent, can be directly calculated [20,21].

Numerous methods are available in the fabrication of Ti-based alloys for different biomedical applications, such as selective laser melting, metal injection molding, electron beam melting, powder metallurgy, etc., owing to their high melting point, contamination susceptibility, and reactivity at high temperature, the Ti alloys are problematic to be formed from casting [13,22]. A foremost hindrance to the usage of titanium-based alloys in numerous probable biomedical uses is that they are expensive, mostly for the accompanying cost of machining, as well as the expense to refine Ti sponges. The usage of the powder metallurgy method is a promising alternative, as it ensures not merely the manufacturing of net-shape components, but similarly, considerably cuts production expenses. It was stated that the usage of powder metallurgy permits achieving a <20% decrease of unused material. Additionally, in 2009 Zhang et al. [22] studied powder metallurgy, the Ti-Mn alloys containing 8 and 12% Mn were designed by spark plasma sintering verified that it promoted the cell adhesion properties. The authors finalized that adding Mn in the Ti matrix might be a reason for the major rise in the Young modulus and hardness of the titanium-based

alloys, although at a similar time decreasing the  $\alpha$  to  $\beta$  transformation temperature. This method offers an additional benefit in that a tougher linking of the implant surface with the nearby tissues can be attained by bone growth onto the porous titanium surface, resulting in enhanced fatigue strength and wholly upgraded biocompatible properties. Because of these reasons, powder metallurgy is a promising route for the production of Ti alloys, as it produces net-shape components [23].

In this research, Ti6Al4V, Ti5Mn, and Ti10Mn alloys are produced by the powder metallurgy method. The main objective of this research is to design a new material for biomedical applications that must not be cytotoxic. To achieve this objective, manganese is selected as an alloying element with titanium as it is low-cost material and its cytotoxicity level is low as compared to aluminum and vanadium. After the production of existing and new alloys via the powder metallurgy method, they were characterized by the nanoindentation method to compare the mechanical properties, such as hardness, elastic modulus, wear resistance of Ti6Al4V, Ti5Mn, and Ti10Mn alloys, in addition to microstructures.

## 2. Materials and Methods

### 2.1. Materials

The materials chosen to do the fabrication of Ti-based alloys for biomedical applications are pure titanium (Ti), aluminum (Al), vanadium (V), and manganese (Mn) powders. Titanium is nominated as a matrix material and manganese is used as an alloying agent.

### 2.2. Methods

Ti6Al4V, Ti5Mn, and Ti10Mn alloys were produced by the powder metallurgy method. The reason behind the selection of manganese concentration is that the Mn < 13 wt% can be utilized to yield noble biocompatible alloys [11]. The first one has 6wt% aluminum and 4 wt% vanadium, the second one has 5 wt% Mn, while the third has 5wt% Mn. Afterward, for all sets of samples, the powders were weighted in an inert atmosphere by using a glove box (TOB-STX2). Each component of the calculated composition was mechanically alloyed for 1 h at 300 rpm to get the homogenized powder via ball milling equipment 4 Tank Mixer (Desktop Vertical Automatic Mixer model, MTI Corporation (Richmond, CA, USA)). Steel balls were selected as grinding media having the ball-to-powder ratio = 15:1. The powders were then compacted by using a die compaction setup with 8000 psi being pressure applied for 300 s. The sintering was performed at 900 °C with a heating rate of 5 °C/min in a vacuum furnace for 3 h. The main aim of the sintering step was to bind the powder particles together and finally produce the sintered alloys.

### 2.3. X-ray Fluorescence

X-ray fluorescence (XRF, ZSX primus, Rigaku, Japan) was used to identify the compositional change in the titanium alloy coupons' surface.

### 2.4. Phase Composition Examination

PANalytical X-pert Pro XRD DY3313 (Eindhoven, the Netherlands) was used for the investigation of the phases present in the developed alloys. The diffracted peaks were noted in the range of 10–80° over  $2\theta$  at a speed of 0.1°/s.

### 2.5. Microstructural Analysis

Sintered samples with finalized dimensions (diameter = 30 mm and height = 6 mm) were manufactured. For microstructural characterization, the samples underwent several steps: (1) the surface was first ground via silicon carbide (SiC) paper (220 to 1200 grade). (2) Samples were then polished followed by washing with acetone and swapping with distilled water. They were then dried out with purified air. (3) Next, the etching of the samples was done via Kroll's reagent to expose its micrograph [24]. (4) The microstructural evaluation of the samples was examined via OM. All experimentations were performed at room temperature.

## 2.6. Relative Density and Porosity

The relative density of all titanium-based alloys was determined via Equation (1) and porosity was calculated using Equation (2), where  $\rho_r$ ,  $\rho_s$  and  $\rho_g$  represent the relative, sintered, and green compact density of alloys, respectively, and  $P_t$  represents the total porosity of alloys:

$$\rho_r = \frac{\rho_g}{\rho_s} \quad (1)$$

$$P_t = 100 \left( 1 - \frac{\rho_s}{\rho_t} \right) \quad (2)$$

## 2.7. Nanoindentation

In this research, nanoindentation tests were executed on an Anton Paar nanoindenter (UHT<sup>3</sup>). A Berkovich indenter (armed with a three-sided pyramid) made of diamond is used to perform the nanoindentation tests. The ultimate goal of this technique is to calculate the penetration depth of an indenter tip against the load applied to a well-polished mirror-like superficial surface of the sample. All the indentation tests were in good agreement with ISO 14577. Preceding the measurement, calibration of the tip was completed on fused silica to conserve accurateness. During the tests, the parameters were as follows: dwell time = 30 sec, loading rate = 1 mN/s, indenter geometry shape factor = 1.0, and maximum load = 50 mN [25]. The hardness,  $H$  is calculated by using Equation (3) [26]:

$$H = \frac{P_{max}}{A} \quad (3)$$

### 2.7.1. Elastic Modulus

$E_r$ , i.e., the reduced elastic modulus, is the sum of the elastic modulus of both the alloys and the indenter tip. This was calculated as per work done by Zhang et al. [22].

### 2.7.2. Yield Pressure and Wear Properties

Yield pressure is the capability of the material to resist plastic deformation after the application of load, and this can be determined by using the ratio of hardness and reduced elastic modulus given in Equation (4):

$$\text{Yield pressure} = \frac{H^3}{E_r^2} \quad (4)$$

At the same time, wear properties of alloys are directly related to the ratio of hardness and elastic moduli and calculated yield pressure values.

## 3. Results

### 3.1. Elemental Analysis

The chemical compositions of titanium, aluminum, manganese, and vanadium powders were determined by using X-ray Fluorescence (XRF). X-ray fluorescence (XRF) is used to analyze the purity of powders that are used in as-received conditions, shown in Table 1.

**Table 1.** The purity level of different powders by using XRF analysis.

Elements	Purity (%)
Ti	98.5
V	99.0
Mn	99.0
Al	99.0

### 3.2. Microstructural Characterization

The microstructure of titanium-based alloys is typically observed in terms of the size, arrangement, and shape of  $\alpha$  and  $\beta$  phases, as represented in Figure 1a–c. In case of Ti-5Mn, equiaxed and elongated grains are perceived, while in the case of Ti-10Mn alloys, equiaxed grains are observed in microstructures.

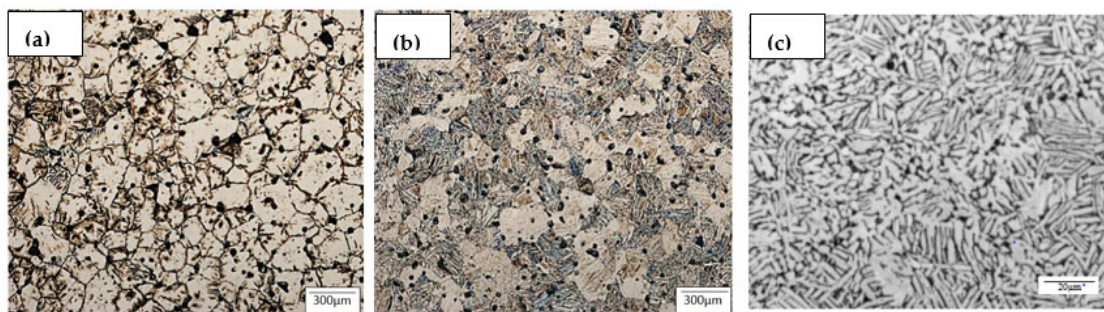


**Figure 1.** (a,b) show the ( $\alpha$ ) alpha and ( $\beta$ ) beta phases of Ti-5Mn and Ti-10Mn alloys ( $400\times$ ), respectively, and (c) shows the optical structure of Ti6Al4V alloy ( $400\times$ ).

### 3.3. Phase Composition Examination

XRD pattern of the titanium-based alloys is presented in Figure 2. The pattern confirms the presence of alpha and beta phases in the Ti5Mn and Ti6Al4V alloys and a beta phase in the Ti10Mn alloy. This result is also in compliance with the work done by Azmat et al. [27].

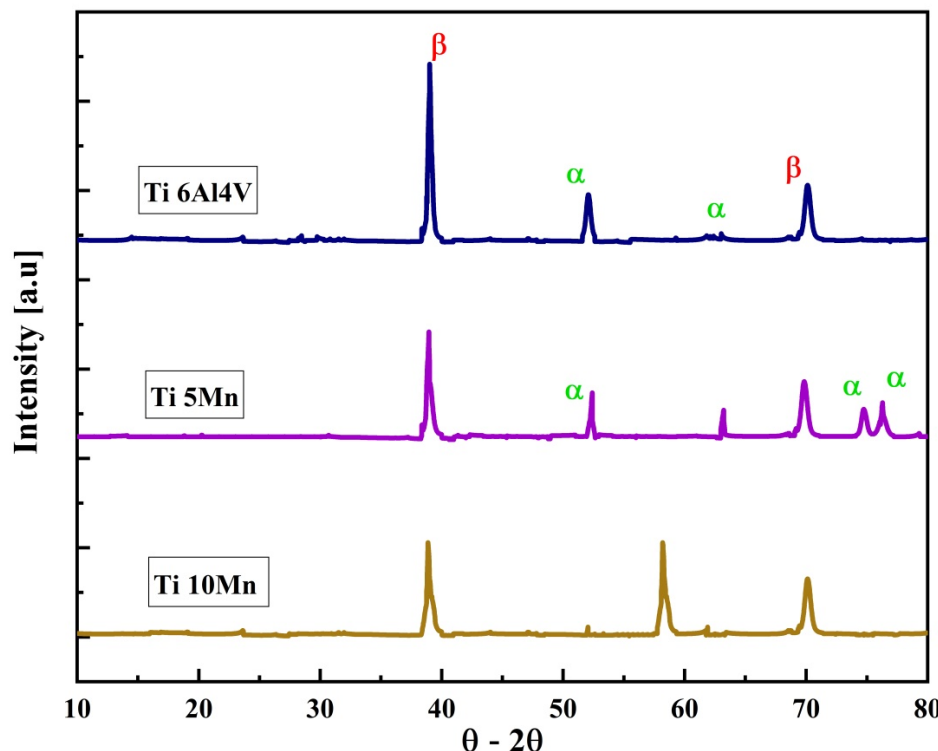


**Figure 2.** The XRD pattern of the titanium-based alloys. The pink line represents Ti5Mn, the brown line represents Ti10Mn, and the blue line represents Ti6Al4V.

### 3.4. Relative Density

Figure 3 presents the relative densities and porosity level of the titanium-based alloys, which were calculated by using Equations (1) and (2). The direct relation of relative densities with the manganese content was observed, which results in a decrease in porosity level, i.e., the densification is maximum.

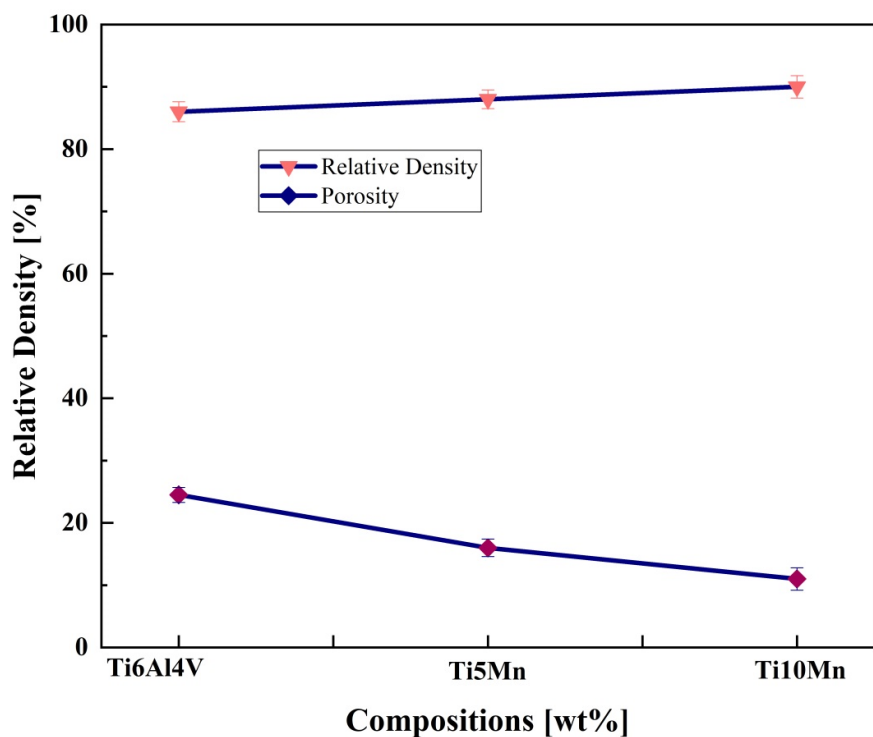


**Figure 3.** The relative density and porosity of the titanium-based alloys.

### 3.5. Nanoindentation

#### 3.5.1. Load versus displacement curves of the Ti6Al4V, Ti-10Mn, and Ti-5Mn alloy

Generally, nanoindentation tests consist of three stages:

1. Loading stage;
2. Holding stage;
3. Unloading stage.

The loading curve further comprises two states: the elastic loading region, which indicates the elastic deformation, and then the plastic loading region, which indicates that the plastic deformation is observed. The second stage is ordinarily used to reveal the deformation process (time-dependent) of indented materials. In the third stage, the elastic recovery process is observed and the Oliver and Pharr (O-P) technique is used to calculate the E and H values [28]. Loading and unloading graphs are shown in Figure 4.

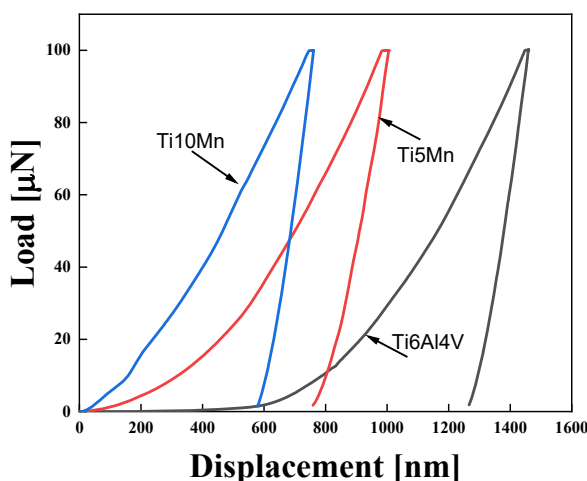


**Figure 4.** The different stages of the load-displacement curve of Ti-5Mn, Ti10Mn, and Ti6Al4V. The blue line represents Ti10Mn, the red line represents Ti5Mn, and the black line represents Ti6Al4V.

### 3.5.2. Nanohardness

Nanoindentation testing is used to determine the hardness value at the maximum load in the load versus displacement curve. The nanohardness values were determined by using Equation (3) and the values of the existing alloy were associated with the new design alloy are shown in Figure 5. The figure shows the comparison of  $\beta$ -phase hardnesses, as it is considered to be important for biomedical applications. Hardness is defined as how resistant a material is when force is applied. Replacement of aluminum and vanadium by manganese revealed an increment in hardness value from 2264.1 MPa to 9109.2 MPa. As there are high chances that indentation at nano-level may have induced work hardening, hence a Vicker hardness test was also performed to compare the hardness of  $\alpha$  and  $\beta$  phases with the bulk sample, and the result is shown in Table 2.

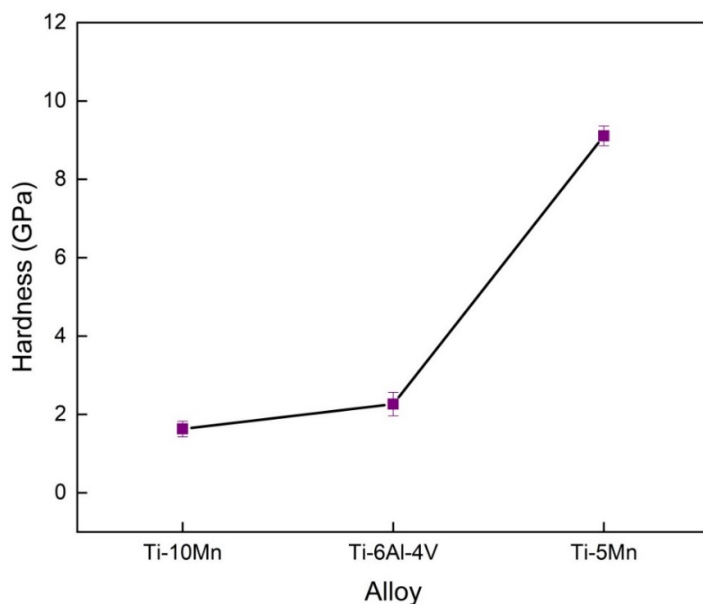


**Figure 5.** The nanohardness of the titanium-based alloys.

**Table 2.** The hardness values of  $\alpha$  and  $\beta$  phases and the bulk sample.

S.No.	Alloys	Nanohardness (MPa)		Vicker's Hardness (MPa)
		$\alpha$ -Phase	$\beta$ -Phase	
1	Ti-5Mn	2056.1	3098.2	450
2	Ti-10Mn	1992.2	2264.1	380
3	Ti-6Al-4V	1908.1	2461.2	335

### 3.5.3. Reduced Elastic Modulus of the Ti6Al4V, Ti-5Mn Alloy, and Ti-10Mn

Figure 6 shows comparatively Ti-5Mn has a high value of elastic modulus. Moreover, the calculated ratio of hardness ( $H$ ) and reduced elastic modulus ( $E_r$ ) values of Ti6Al4V and Ti5Mn helps find the elastic behavior limit and also has an effect on the wear behavior of the alloy.

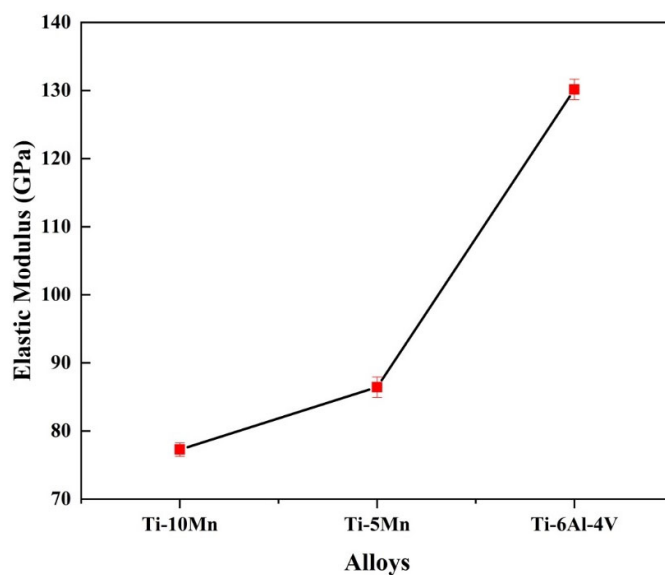


**Figure 6.** The reduced elastic modulus of the titanium-based alloys.

### 3.5.4. Yield Pressure and Wear Properties

Figure 7 shows the comparative values of  $H/E_r$  and  $H^3/E_r^2$  ratios for all alloys, calculated by using Equation (4). Ti-5Mn has a high value of yield pressure (resistance to plastic deformation in the presence of load) and an  $H/E_r$  ratio. The enhancement in hardness (HIT) and reduced elastic modulus ( $E_r^2$ ) value of Ti-5Mn shows enhanced wear resistance and resistance to plastic deformation.

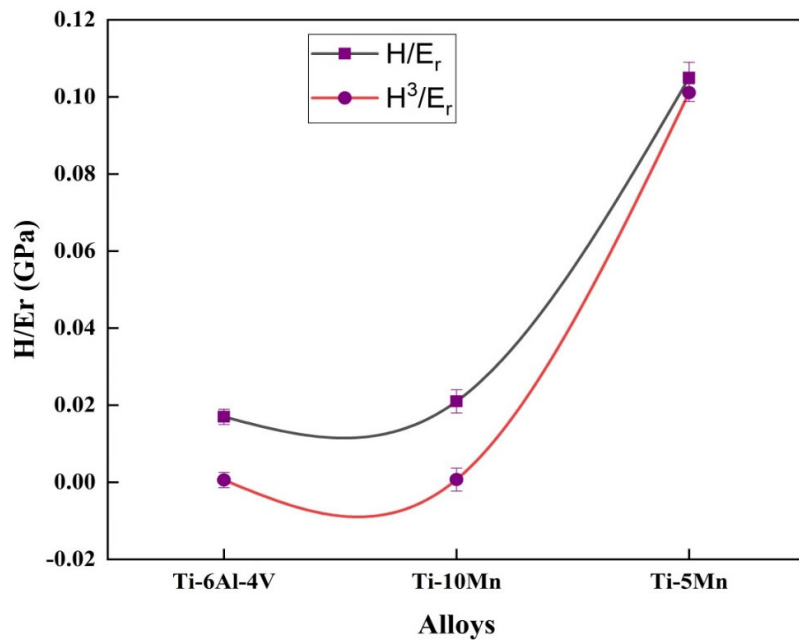


**Figure 7.** The yield pressure and wear properties of the titanium-based alloys.

## 4. Discussions

### 4.1. Elemental Analysis

The results show that powder is of high purity and this powder purity is directly related to the mechanical and biomedical properties of the finished alloys.

#### 4.2. Microstructure

The optical micrograph of the sintered Ti6Al4V revealed the dual phases containing alternating layers of  $\alpha$  and  $\beta$  phases, as illustrated in Figure 1c. The lamellar microstructure is linked with strength because of the  $\alpha$  phase size that affects inferior ductility, which is also verified by Nalla and co-workers [29].

The optical image of Ti-5Mn alloy is characterized as equiaxed and elongated grains and shown in Figure 1a. The amount of  $\beta$  lamella grows in quantity, and the interlamellar spacing declines as the Mn content rises from 5 to 10%. Ti10Mn consists of equiaxed  $\beta$  phase grains (Figure 1b), while thin extended grains are observed at the grain boundaries and inside the few grains. Certainly, no clusters of powders were observed, and therefore, the homogeneous microstructures are achieved, which was not related to the addition of the manganese powder percentage. The quantity of  $\beta$  lamella is dependent on the Mn content; it increases in number as well as abundance, but at the same time, the interlamellar spacing reduces with the increase in Mn amount. Regarding the micro constituents, the Ti5Mn and Ti10Mn microstructures are composed of equiaxed and extended grains [30].

Generally, after the addition of Mn powder, the  $\beta$  phase stabilizes and its quantity uniformly rises [31]. Ti5Mn has the characteristic lamellar structure of both  $\alpha$  and  $\beta$  phases due to the large quantity of  $\beta$  stabilizer, i.e., Mn incorporated into the Ti matrix.

#### 4.3. Phase Composition Analysis

Referring to the XRD patterns in Figure 2, the Ti5Mn and Ti6Al4V alloys contained both alpha and beta phases, whereas only the beta phase is observed in the case of Ti10Mn alloy, which confirms that the beta phase of the alloy increases with the increase in manganese content. This is because manganese stabilizes the  $\beta$ -phase [10,32].

In Ti5Mn, the amount of beta lamella is influenced by the amount of Mn; as the Mn content rises, it becomes more numerous and rich, but at the same time, the interlamellar phase shrinks [33]. In comparison to Ti6Al4V, Ti5Mn contains a higher amount of a  $\beta$  stabilizer, which gives it the typical lamellar structure of both  $\alpha$  and  $\beta$  phases [34,35].

#### 4.4. Relative Density

The deviation of the relative density of the sintered binary TiMn alloys and Ti6Al4V alloys is shown in Figure 3. In total, 91% of relative density was observed by using a vacuum furnace during the sintering process, which shows that the density of alloys is directly related to the content of manganese. The homogeneity was confirmed via EDS examination, which specified the chemical composition in wt% of alloys, i.e., 99.07Ti-0.93Mn, 94.98Ti-5.02Mn, and 90.54Ti-9.46Mn. Ti5Mn alloys are categorized by a  $\alpha + \beta$  lamellar microstructure (Figure 3) [11].

#### 4.5. Nanoindentation

Figure 4 reveals the load (P) versus displacement (h) curve of Ti5Mn, Ti10Mn, and Ti6Al4V, respectively, obtained during the nanoindentation tests. For all the specimens, the P versus h curve was observed to be smooth, but in the case of Ti5Mn, there was a considerable decrease in depth. The decrease specifies an increment in the hardness value of the newly designed alloy. Generally, the load-displacement curve depends on several factors, such as the force applied, the material onto which testing will be done, and environmental conditions during nanoindentation testing. Overall different materials possess different shapes of load versus displacement curves, and in this research, the curve profile shows that the material performs in both elastic and plastic mode. The reason behind the shifting of curves towards the left indicates that among all alloys, Ti5Mn efficiently reduced the displacement from 1200 to 600 (in the case of Ti6Al4V) because of the strengthening mechanism and load sharing capability. The Ti5Mn curve shows the least displacement, although Ti6Al4V indicates the uppermost maximum displacement and the maximum elastic modulus of 130.13 GPa. The gradient of unloading and modulus are strictly connected to the stiffness, which results in an increase in the modulus of elasticity.

The loading part of the P versus h curve joins the complex reaction of the material to strain including elastic, although the unloading part of the curve for maximum materials contains mostly elastic recovery [36,37].

#### 4.6. Nanohardness

The outcomes of the hardness testing show that the hardness of sintered samples is inversely related to the addition of Mn content, as it was observed that the hardness decreases from 180.0 to 336.7 MPa with the increase in Mn content. This is due to the formation of the  $\omega$  phase in Ti-5Mn alloy and the effect of solid solution strengthening decreases with the increase in Mn content (Figure 5).

#### 4.7. $E_r$ of the Ti6Al4V, Ti-5Mn Alloy, and Ti-10Mn

Solid solution hardening has an impact on both the hardness and elastic modulus properties of Ti(5–10)Mn, which is due to the presence of Mn and the quantity of the  $\omega$  phase, a thermal in the alloys. Contrarily, the volume section of the omega ( $\omega$ ) phase decreases with an increase in Mn content, which results in a reduction in both nanohardness and Young's modulus properties [24], as shown in Figure 6.

#### 4.8. Yield Pressure and Wear Properties

Enhanced wear properties (Figure 7) and yield pressure are significant features for biomedical applications, since dental implants are typically exposed to wear with the surrounding bone. Therefore, superior wear resistance can diminish the creation of wear debris that causes nontoxic reactions, resulting in implant loosening and the required modification in surgery. Ti-5Mn has high hardness as well as high wear properties. This is because the addition a minimum amount of Mn in a Ti-based alloys results in enhanced wear properties of the newly developed alloys [38].

### 5. Conclusions

In the current research, manganese was selected as a  $\beta$  stabilizer to produce novel Ti-based alloys for biomedical usages, such as dental implants orthopedic applications, etc., at minimal expense. Cost declination depends not only on the selection of the alloying elements but also on the selection of the manufacturing route. Especially, this research validates that Ti-based alloys can fruitfully be produced via the powder metallurgy route. Based on the present set of experimental conditions, we provide some concluding remarks. Manganese addition has a profound effect on the hardness, elastic modulus, and microstructure of the alloy. Comparatively, the Ti5Mn alloy exhibits enhanced hardness and elastic modulus. However, a Ti5Mn alloy with 5 wt% Mn is suggested to be the best replacement for aluminum and vanadium for cell implantology because of high hardness and lower elastic modulus and wear properties. To conclude, the nanoindentation load can be properly adjusted to determine the mechanical properties as compared to conventional mechanical tests. It was also observed that nanoindentation can be used to measure the wear properties of the PM-fabricated Ti6Al4V, Ti5Mn, and Ti10Mn alloys.

**Author Contributions:** Conceptualization, A.D.C.; methodology, A.A. (Ambreen Azmat). and S.A.; writing, I.A.C., F.S. and J.A.; validation, I.A.C. and A.D.C.; investigation, J.A., I.A.C., S.A. and S.F.; supervision, A.D.C.; funding acquisition, M.A.S. and A.A. (Abdulaziz AlHazaa). All authors have read and agreed to the published version of the manuscript.

**Funding:** This research was funded by the Researcher's Supporting Project Number (RSP-2021/269), King Saud University, Riyadh, Saudi Arabia.

**Institutional Review Board Statement:** Not applicable.

**Informed Consent Statement:** Not applicable.

**Data Availability Statement:** Data are available upon request from the corresponding authors.

**Acknowledgments:** The authors would like to acknowledge the Researcher’s Supporting Project Number (RSP-2021/269), King Saud University, Riyadh, Saudi Arabia, for their support of this work.

**Conflicts of Interest:** The authors declare that they have no known competing financial interests or personal relationships that could have appeared to influence the work reported in this paper.

## References

1. Rodriguez, G.M.; Bowen, J.; Zelzer, M.; Stamboulis, A. Selective modification of Ti6Al4V surfaces for biomedical applications. *RSC Adv.* **2020**, *10*, 17642–17652. [\[CrossRef\]](#) [\[PubMed\]](#)
2. Fuller, R.; Landrigan, P.J.; Balakrishnan, K.; Bathan, G.; Bose-O'Reilly, S.; Brauer, M.; Caravanos, J.; Chiles, T.; Cohen, A.; Corra, L.; et al. Pollution and health: A progress update. *Lancet Planet. Health* **2022**, *6*, e535–e547. [\[CrossRef\]](#)
3. Asrar, S.; Tufail, M.; Chandio, A.D. Facile Coating of HAP on Ti6Al4V for Osseointegration. *Eng. Technol. Appl. Sci. Res.* **2021**, *11*, 7240–7246. [\[CrossRef\]](#)
4. Khadija, G.; Saleem, A.; Akhtar, Z.; Naqvi, Z.; Gull, M.; Masood, M.; Mukhtar, S.; Batool, M.; Saleem, N.; Rasheed, T.; et al. Short term exposure to titanium, aluminum and vanadium (Ti 6Al 4V) alloy powder drastically affects behavior and antioxidant metabolites in vital organs of male albino mice. *Toxicol. Rep.* **2018**, *5*, 765–770. [\[CrossRef\]](#) [\[PubMed\]](#)
5. Kawahara, M.; Kato-Negishi, M. Link between Aluminum and the Pathogenesis of Alzheimer's Disease: The Integration of the Aluminum and Amyloid Cascade Hypotheses. *Int. J. Alzheimer's Dis.* **2011**, *2011*, 276393. [\[CrossRef\]](#)
6. Zhang, F.; Weidmann, A.; Nebe, J.B.; Beck, U.; Burkhardt, E. Preparation, microstructures, mechanical properties, and cytocompatibility of TiMn alloys for biomedical applications. *J. Biomed. Mater. Res. Part B Appl. Biomater.* **2010**, *94*, 406–413. [\[CrossRef\]](#)
7. Si, J.; Lv, Y.; Lu, S.; Xiang, Y. Microscopic phase-segregated quaternary ammonia polysulfone membrane for vanadium redox flow batteries. *J. Power Sources* **2019**, *428*, 88–92. [\[CrossRef\]](#)
8. Alqattan, M.; Peters, L.; Alshammari, Y.; Yang, F.; Bolzoni, L. Antibacterial Ti-Mn-Cu alloys for biomedical applications. *Regen. Biomater.* **2021**, *8*, rbaa050. [\[CrossRef\]](#)
9. Della Pepa, G. Microelements for bone boost: The last but not the least. *Clin. Cases Miner. Bone Metab.* **2016**, *13*, 181–185. [\[CrossRef\]](#)
10. Santos, P.F.; Niinomi, M.; Liu, H.; Cho, K.; Nakai, M.; Itoh, Y.; Narushima, T.; Ikeda, M. Fabrication of low-cost beta-type Ti-Mn alloys for biomedical applications by metal injection molding process and their mechanical properties. *J. Mech. Behav. Biomed. Mater.* **2016**, *59*, 497–507. [\[CrossRef\]](#)
11. Alshammari, Y.; Yang, F.; Bolzoni, L. Mechanical properties and microstructure of Ti-Mn alloys produced via powder metallurgy for biomedical applications. *J. Mech. Behav. Biomed. Mater.* **2019**, *91*, 391–397. [\[CrossRef\]](#)
12. Attar, H.; Ehtemam-Haghghi, S.; Kent, D.; Okulov, I.; Wendrock, H.; Bönisch, M.; Volegov, A.; Calin, M.; Eckert, J.; Dargusch, M. Nanoindentation and wear properties of Ti and Ti-TiB composite materials produced by selective laser melting. *Mater. Sci. Eng. A* **2017**, *688*, 20–26. [\[CrossRef\]](#)
13. Abro, S.H.; Chandio, A.; Siddiqui, M.A.; Channa, I.A. Aluminum and aluminum nitrides effect on nucleation sites in micro-alloyed steel. *Proc. Pakistan Acad. Sci. Part B* **2019**, *56*, 17–26.
14. Makhdoom, M.A.; Sgobba, V.; Channa, I.A.; Ghewins, N. Producing oxide free silicon nanocrystals—A novel & benign approach. *Optik* **2021**, *246*, 167789. [\[CrossRef\]](#)
15. Giraldez, I.; Garrido, M.; Río, T.; Ceballos, L.; Rodriguez, J. Comparison of the mechanical properties of dentin and enamel determined by different nanoindentation techniques: Conventional method and continuous stiffness measurement. *Boletín Soc. Española Cerámica Vídr.* **2010**, *49*, 177–182.
16. Tuninetti, V.; Jaramillo, A.F.; Riu, G.; Rojas-Ulloa, C.; Znaidi, A.; Medina, C.; Mateo, A.M.; Roa, J.J. Experimental Correlation of Mechanical Properties of the Ti-6Al-4V Alloy at Different Length Scales. *Metals* **2021**, *11*, 104. [\[CrossRef\]](#)
17. Radhakrishnan, P.M.; Dheepthi, M. A Review on Nano-Indentation of Thin Polymeric Films. *Int. J. Eng. Res. Technol.* **2019**, *8*, IJERTV8IS030084.
18. Ashfaq, J.; Channa, I.A.; Shaikh, A.A.; Chandio, A.D.; Shah, A.A.; Bughio, B.; Birmahani, A.; Alshehri, S.; Ghoneim, M.M. Gelatin-and Papaya-Based Biodegradable and Edible Packaging Films to Counter Plastic Waste Generation. *Materials* **2022**, *15*, 1046. [\[CrossRef\]](#)
19. Bull, S.J. Nanoindentation of coatings. *J. Phys. D Appl. Phys.* **2005**, *38*, R393–R413. [\[CrossRef\]](#)
20. Ragupathy, S.; Priyadharsan, A.; AlSalhi, M.S.; Devanesan, S.; Guganathan, L.; Santhamoorthy, M.; Kim, S. Effect of doping and loading Parameters on photocatalytic degradation of brilliant green using Sn doped ZnO loaded CSAC. *Environ. Res.* **2022**, *210*, 112833. [\[CrossRef\]](#)
21. Ahmad, S.; Channa, I.A. Mathematical Relationship between Ferritic, Pearlitic and Average Grain Size of Steel. *J. Mod. Sci. Technol.* **2013**, *1*, 1–18.
22. Chen, L.-Y.; Cui, Y.-W.; Zhang, L.-C. Recent Development in Beta Titanium Alloys for Biomedical Applications. *Metals* **2020**, *10*, 1139. [\[CrossRef\]](#)
23. Ehtemam-Haghghi, S.; Cao, G.; Zhang, L.-C. Nanoindentation study of mechanical properties of Ti based alloys with Fe and Ta additions. *J. Alloys Compd.* **2016**, *692*, 892–897. [\[CrossRef\]](#)

24. Santos, P.F.; Niinomi, M.; Cho, K.; Nakai, M.; Liu, H.; Ohtsu, N.; Hirano, M.; Ikeda, M.; Narushima, T. Microstructures, mechanical properties and cytotoxicity of low cost beta Ti–Mn alloys for biomedical applications. *Acta Biomater.* **2015**, *26*, 366–376. [[CrossRef](#)] [[PubMed](#)]
25. Wen, Y.; Xie, L.; Wang, Z.; Wang, L.; Lu, W.; Zhang, L.-C. Nanoindentation characterization on local plastic response of Ti-6Al-4V under high-load spherical indentation. *J. Mater. Res. Technol.* **2019**, *8*, 3434–3442. [[CrossRef](#)]
26. Li, R.; Riester, L.; Watkins, T.; Blau, P.J.; Shih, A.J. Metallurgical analysis and nanoindentation characterization of Ti-6Al-4V workpiece and chips in high-throughput drilling. *Mater. Sci. Eng. A* **2008**, *472*, 115–124. [[CrossRef](#)]
27. Azmat, A.; Tufail, M.; Chandio, A.D. Synthesis and Characterization of Ti-Sn Alloy for Orthopedic Application. *Materials* **2021**, *14*, 7660. [[CrossRef](#)]
28. Si, Y. Effect of Manganese Addition on the Microstructure and Mechanical Properties of Ti-Nb Biomedical Alloys. *IOP Conf. Ser. Earth Environ. Sci.* **2019**, *252*, 022137. [[CrossRef](#)]
29. Maja, M.E.; Falodun, O.E.; Obadele, B.A.; Oke, S.R.; Olubambi, P.A. Nanoindentation studies on TiN nanoceramic reinforced Ti-6Al-4V matrix composite. *Ceram. Int.* **2018**, *44*, 4419–4425. [[CrossRef](#)]
30. Almanza, E.; Pérez, M.; Rodríguez, N.; Murr, L. Corrosion resistance of Ti-6Al-4V and ASTM F75 alloys processed by electron beam melting. *J. Mater. Res. Technol.* **2017**, *6*, 251–257. [[CrossRef](#)]
31. Dalmau, A.; Pina, V.G.; Devesa, F.A.; Amigó, V.; Muñoz, A.I. Electrochemical behavior of near-beta titanium biomedical alloys in phosphate buffer saline solution. *Mater. Sci. Eng. C* **2015**, *48*, 55–62. [[CrossRef](#)] [[PubMed](#)]
32. Waheed, H.; Hussain, A.; Farrukh, S. Fabrication, characterization and permeation study of ultrafiltration dialysis membranes. *Desalination Water Treat.* **2016**, *57*, 24799–24806. [[CrossRef](#)]
33. Santos, P.F.; Niinomi, M.; Liu, H.; Nakai, M.; Cho, K.; Narushima, T.; Ueda, K.; Ohtsu, N.; Hirano, M.; Itoh, Y. Development and Performance of Low-Cost Beta-Type Ti-Based Alloys for Biomedical Applications Using Mn Additions BT. In *Interface Oral Health Science 2016*; Springer: Singapore, 2017; pp. 229–245.
34. Ran, J.; Jiang, F.; Sun, X.; Chen, Z.; Tian, C.; Zhao, H. Microstructure and Mechanical Properties of Ti-6Al-4V Fabricated by Electron Beam Melting. *Crystals* **2020**, *10*, 972. [[CrossRef](#)]
35. Ikeda, M.; Ueda, M.; Kinoshita, T.; Ogawa, M.; Niinomi, M. Influence of Fe Content of Ti-Mn-Fe Alloys on Phase Constitution and Heat Treatment Behavior. *Mater. Sci. Forum* **2012**, *706–709*, 1893–1898. [[CrossRef](#)]
36. Voyiadjis, G.Z.; Yaghoobi, M. Review of Nanoindentation Size Effect: Experiments and Atomistic Simulation. *Crystals* **2017**, *7*, 321. [[CrossRef](#)]
37. Majumdar, P.; Singh, S.; Chakraborty, M. Elastic modulus of biomedical titanium alloys by nano-indentation and ultrasonic techniques—A comparative study. *Mater. Sci. Eng. A* **2008**, *489*, 419–425. [[CrossRef](#)]
38. Pascu, C.I.; Gheorghe, S.; Rotaru, A.; Nicolicescu, C.; Cioateřă, N.; Roșca, A.S.; Sârbu, D.; Rotaru, P. Ti-based composite materials with enhanced thermal and mechanical properties. *Ceram. Int.* **2020**, *46*, 29358–29372. [[CrossRef](#)]